Transfer Function Method to Diagnose Axial Displacement and Radial Deformation of Transformer Windings

Ebrahim Rahimpour, Jochen Christian, Kurt Feser, *Fellow, IEEE,* and Hossein Mohseni

***Abstract*—Short circuit currents or forces during transport can cause mechanical displacements of transformer windings. The transfer function method is presented as a tool to detect these displacements. In order to be able to evaluate the measurements, the correlation between the characteristics of transfer functions and possible damages must be known. Axial displacement and radial deformation of transformer windings have been studied in this research work using two test transformers. The primary winding of the first transformer for axial displacement has 31 double disk coils (1.3 MVA, 10 kV) and the secondary winding is a four layer winding. The second transformer for the study of radial deformation has 30 double disk coils (1.2 MVA, 10 kV) as primary winding and a one layer winding as secondary winding. The detailed mathematical models were developed for the test objects and a comparison was carried out between measured and calculated results. It is shown that this model can present the behavior of the transformer windings in the frequency domain in the case of sound and displaced conditions.**

***Index Terms*—Diagnose, mechanical displacements, modeling, transfer function, transformer windings.**

I. Introduction

THE aim of modern monitoring and diagnostic methods is to ensure the optimal and reliable utilization of transformers in respect to the transferred power and its life time. In this regard several procedures such as thermal monitoring, oil analyzes (Dissolved Gas Analyzes, Furfurol), partial discharge measurements (electric, acoustic), transfer function, relaxation current, recovery voltage measurement, etc., are investigated and applied. Each method can be applied for a specific type of problem and has its own merits. Transfer function variations are used as a tool to recognize mechanical displacements and deformation of windings [1], but determining the exact location and the extent of these faults are subject to active research. The suitability of this method was confirmed in several experiments on power transformers in service [2], [3].

The high frequency behavior of windings is characterized by their resonances (transfer maxima) and their transfer minima. Mechanical displacements will change these characteristic properties. This change is much more obvious in the frequency domain than in the time domain (e.g., comparison of two different LVI traces).

This method is a comparative method, i.e., the measurement results should be compared with reference results. If significant deviations in the results occur, the transformer is faulty and appropriate action have to be undertaken. From the operation point of view, the type and the location of the fault are important. The correlation between the faults and the transfer function variations are not clearly known. These relations can be obtained by measurements on power transformers or by developing an appropriate model of the transformer for simulations.

The modeling of a complex arrangement such as a transformer active part is a compromise between accuracy and complexity. The number of definable basic elements and thus the accuracy of the modeling are limited. Between different proposed models, the following classification can be used:

- Black-Box models:
  - Modal analyze based modeling [4]
  - Description by pole and zeros [5]
- Physical models:
  - n-phase transmission line model [6]
  - Detailed model:
- Modeling based on self and mutual inductance [7]
- Modeling based on leakage inductance [8]
- Modeling based on the principle of duality [9]
- Modeling based on electromagnetic fields [10]
- Hybrid model
  - Combination of Black-Box and physical model [11]

The Black-Box models are not suitable for the modeling of winding displacements, since they present just the behavior of the transformer on its terminals. The physical models are based on the geometry of the winding and its lumped equivalent circuit. These models are also valid for higher frequencies.

The modeling of windings by the lumped RL-C-M network (the detailed model) enables the calculation of the currents and voltages using common electrical network analysing tools (e.g., ATP, Pspice, etc.). In addition, it is possible to consider nonlinearities (e.g., hysteresis, saturation) and frequency dependent effects (e.g., eddy current, dielectric losses). Complex windings can be modeled with several coils, which is not possible for the multi-phase transmission line model.

Investigations show that among different approaches of the detailed modeling, the one, which is based on the self and mutual inductance is the most appropriate for the description of the

Manuscript received December 19, 2000; revised December 15, 2001. This work was supported by the German Academic Exchange Service (DAAD).

E. Rahimpour is with the Institute of Power Transmission and High Voltage Technology, University of Stuttgart, D-70569, Germany, on leave from the Electrical Engineering Department, Faculty of Engineering, Tehran University, 14399, Iran.

J. Christian and K. Feser are with the Institute of Power Transmission and High Voltage Technology, University of Stuttgart, D-70569, Germany.

H. Mohseni is with the Electrical Engineering Department, Faculty of Engineering, Tehran University, 14399, Iran.

Digital Object Identifier 10.1109/TPWRD.2003.809692

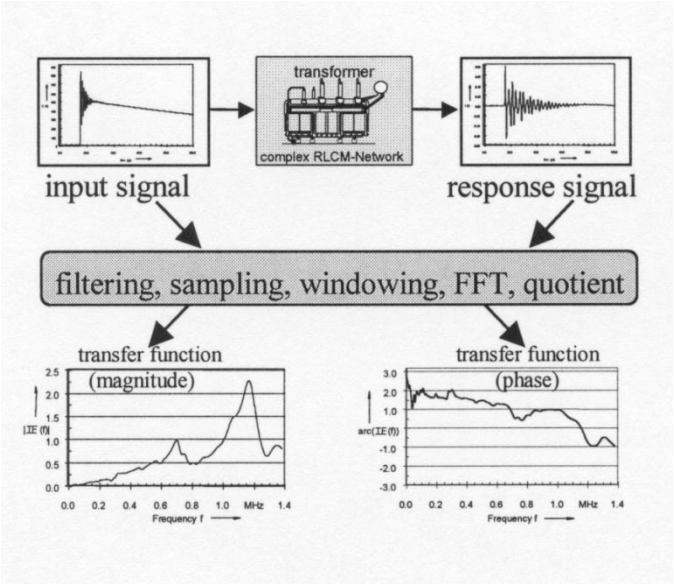

Fig. 1. Measuring the transfer function in the time domain.

magnetic field behavior [12]. Therefore, this model was applied in [13] and it was shown that:

- The detailed R-L-C-M model is determined exclusively from the geometrical dimensions and its validity is sufficient for the frequency range of a few kHz up to approx. 1 MHz.
- The description based on the winding's geometry enables a simple consideration of the dielectric failures in the winding and the determination of the failure location.

This model is used in Sections II–V for the study of axial displacement and radial deformation in transformer windings, to show the ability of the transfer function method as a monitoring tool to detect winding displacements.

II. Measuring Methodology

It is possible to determine the transfer function either by using time or frequency domain measurements. The possible accuracy of both procedures is equal [14]. In the presented investigation all measurements were executed in the time domain. Fig. 1 illustrates the principle of the measurement procedure.

In the time domain, test objects are excited by low or high impulse voltages. The input and output transients are measured and analyzed.

In low voltage measurements the amplitudes are usually 100 V to 2000 V. The shape of the impulse voltage depends on the test device and the test set-up. The bandwidth of the exciting signal should be as high as possible. Typical parameters of the impulse shapes are front times of 100 ns to 500 ns and time to half values of 40 to 200 μs. The spectral distribution of the time domain signals are calculated using FFT. The quotient of output to input signal represents the transfer function in the frequency domain [1].

As a test object for the study of axial displacement a high voltage winding with 31 double inverted disks, 6 turns in each disk, and a four layer concentric low voltage winding, 99 turns each layer, were used. These particular windings were manufactured for special experimental purposes and have the construction of transformer windings with a rated voltage of approx. 10 kV and a rated output of 1.3 MVA. The special construction of the arrangement permits a gradual axial movement of the internal layer winding with respect to the outer winding. The test object has 82.7 cm height and therefore a 1cm axial displacement is equal to 1.2%.

TABLE I
The Degrees of Radial Deformation

Degree of Radial Deformation	Description
Degree 1	The sixth up to the 54th coil were all radially deformed on one side. Deformation was around 7% of the coil radius.
Degree 2	The sixth up to the 54th coil were all radially deformed on two opposite sides. Deformation was around 7% of the coil radius.
Degree 3	The sixth up to the 54th coil were all radially deformed on three sides with 90° with respect to each another. Deformation was around 7% of the coil radius.
Degree 4	The sixth up to the 54th coil were all radially deformed on four sides with 90° with respect to each another. Deformation was around 7% of the coil radius.

As a test object for the study of radial deformation a high voltage winding with 30 double inverted disks, 11 turns in each disk, and a one layer low voltage winding with 23 turns were used. The double disk winding has a rated voltage of 10 kV and a rated output of 1.2 MVA. The deformation has been performed on the double disk winding in four degrees, as tabulated in Table I.

In both studies, the test arrangement was in an oil-immersed cylindrical tank. The equipotential surface establishment for the iron core in both test objects was simulated with a slit cylinder. Fig. 2 illustrates the laboratory arrangements.

To investigate the sensitivity of transfer function measurements for axial displacement and radial deformation, four different terminal conditions have been studied, as shown in Fig. 3.

III. Detailed Model (Based on Self and Mutual Inductance) and Calculation of Its Parameters

The equivalent circuit diagram of the test objects beyond 10 kHz is shown in Fig. 4. A winding unit can contain one disk, two disks or several numbers of turns. The number of units is a modeling parameter and the chosen value is a compromise between the accuracy and the complexity. For the sake of simplicity only three winding units of the double disk high voltage winding are shown in Fig. 4. Only one layer with three winding units have been shown for the low voltage winding in Fig. 4, too.

The elements of the circuit diagram are defined in [13]. Using this model, it is possible to calculate node voltages and branch currents in the time as well as in the frequency domain. Due to the frequency dependence behavior of the resistive elements (Rp_i, Re_i and Rs_i) the calculation in the frequency domain is preferable.

Model parameters are calculated analytically after some simplifications of the geometrical structure of the winding.

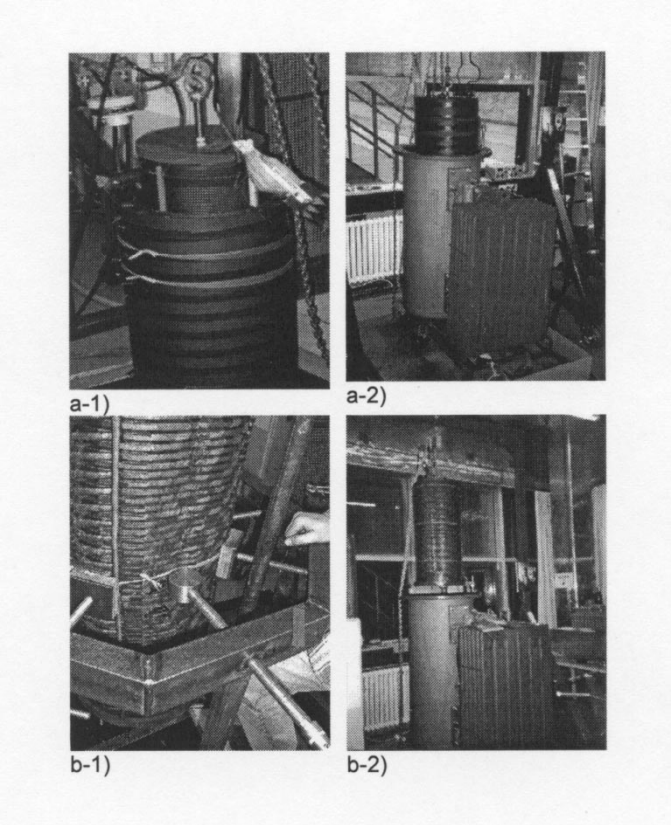

Fig. 2. Laboratory arrangement (One) study of axial displacement: (1) LV and HV windings axial shifted (2) axial shifted windings mounting in the tank (Two) study of radial deformation: (1) mechanical devise for radial deformation (2) LV and radial deformed HV windings mounting in the tank.

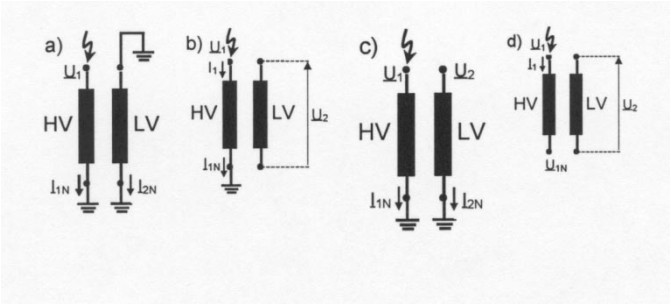

Fig. 3. Different terminal conditions to study the sensitivity of transfer function measurements.

A. Self and Mutual Inductance

The self and mutual inductance can be calculated by the solution of third and fourth Maxwell's equations or vector potential method.

The calculation of the mutual inductance of the arrangement as sketched in Fig. 5 is explained in [15], [16]:

$$M_{12} = \frac{\mu_0}{4\pi} \oint_{C_1} \oint_{C_2} \frac{d\vec{s}_1 \cdot d\vec{s}_2}{R_{12}}. \tag{1}$$

This relation indicates that both integrals must be integrated over the full circumference of both conductors. The integration is executed as follows:

$$M_{12} = \frac{\mu_0}{4\pi} \int_0^{2\pi} \int_0^{2\pi} \frac{r_1(\alpha_1) \cdot r_2(\alpha_2) \cdot \cos(\alpha_2 - \alpha_1)}{R_{12}(\alpha_1, \alpha_2)} \cdot d\alpha_1 \cdot d\alpha_2. \tag{2}$$

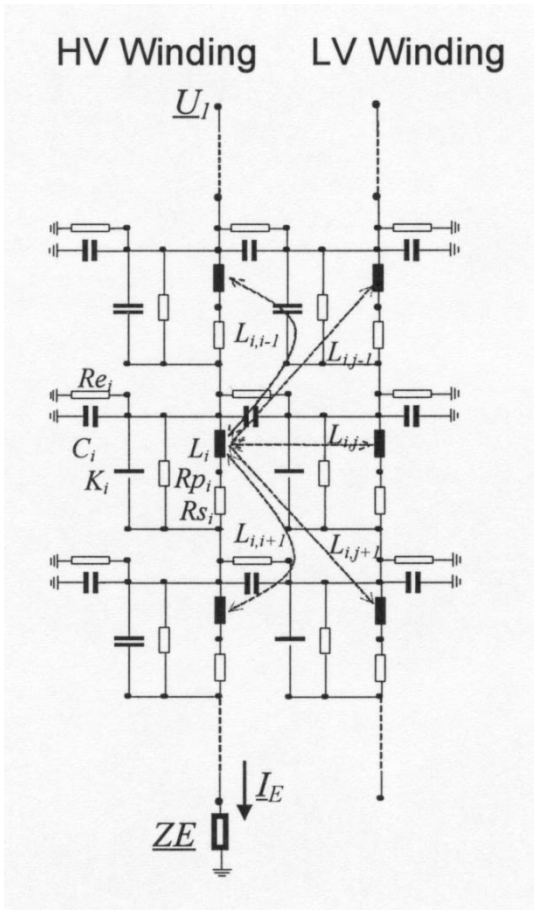

Fig. 4. Detailed model of the test object.

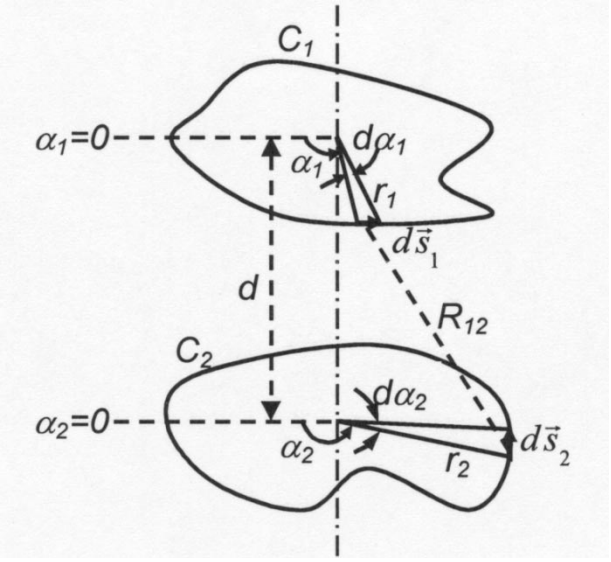

Fig. 5. Two parallel conducting loops.

All parameters in (1) and (2) were shown in Fig. 5. The double integral in (2) is calculated with the help of the numeric trapezoidal rule [17] for the interesting deformed turns. For un-deformed turns, the analysis of (2) results in a closed formula [16], [18]:

$$M_{12} = \frac{2\mu_0\sqrt{r_1 r_2}}{\sqrt{k'}} \cdot [K(k') - E(k')] \tag{3}$$

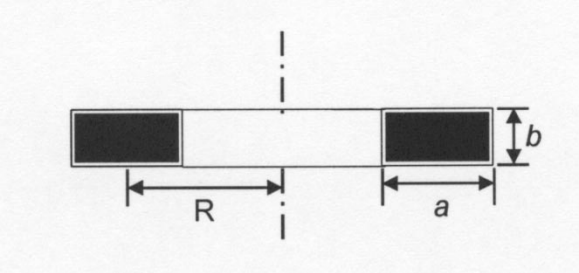

Fig. 6. Definition of the parameters of a turn.

where:

$$k' = \frac{1-\sqrt{1-k^2}}{1+\sqrt{1-k^2}}, \quad k = \sqrt{\frac{4r_1r_2}{(r_1+r_2)^2+d^2}}$$

$K(k')$ and $E(k')$ are the first and second kind of the complete elliptical integrals. r_1 and r_2 are in this case the radii of the interesting turns.

The self inductance of a deformed turn, whose geometry is indicated in Fig. 6, is calculated as mutual inductance of two turns that have the same deformation as the interesting turn. The vertical distance d of the two turns of this equivalent arrangement is called Geometrical Mean Distance (GMD) which can be calculated as [16]:

$$\ln\frac{GMD}{\sqrt{(a^2+b^2}} = \frac{2b}{3a}\tan^{-1}\frac{a}{b} + \frac{2a}{3b}\tan^{-1}\frac{b}{a} - \frac{b^2}{12a^2}\ln\left(1+\frac{a^2}{b^2}\right) - \frac{a^2}{12b^2}\ln\left(1+\frac{b^2}{a^2}\right) - \frac{25}{12}. \quad (4)$$

For a un-deformed turn, the self inductance is calculated with the help of (5)[16], [18].

$$L_i =_0 R\left(\ln\frac{8R}{GMD} - 2\right). \quad (5)$$

The mutual inductance between two winding units with the numbers of turns n_a and n_b can be calculated by summing of the mutual inductances between each turn of unit a and each turn of unit b that are determined with the help of (2) or (3). Therefore $n_a \times n_b$ mutual inductances must be summed [19].

B. Capacitance

Parallel capacitance C_i presents the electrical field between individual disk units and earth (tank or core) as well as the electrical field between different windings.

Considering the dimension of the windings, the calculation of capacitance C_i can be done based on a cylindrical or a homogeneous distribution of the electrical field, if the winding is not deformed. However, an appropriate correction factor is necessary for the edge effects.

For the deformed case, in which the electrical field is inhomogeneous (Fig. 7(a)), the earth capacitance C_i was calculated as total of section capacitances, whose field may be considered homogeneous. Fig. 7(b) shows the idea with the calculation of the capacitance between low voltage winding and high voltage

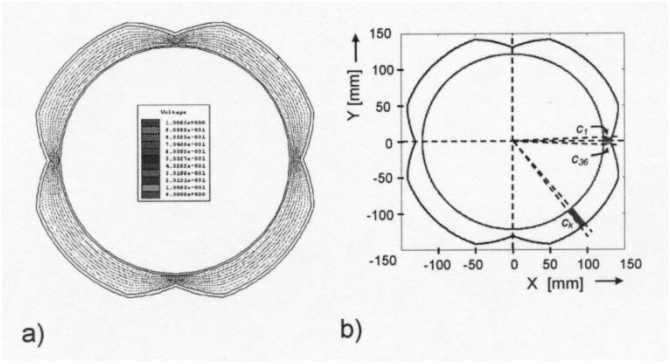

Fig. 7. (a) The distribution of voltage between deformed and not deformed windings, calculated with help of finite element method. (b) The method for the calculation of the capacitances between deformed winding and un-deformed winding or earth.

TABLE II
THE CALCULATED CAPACITANCE BETWEEN TWO WINDINGS OF THE TEST TRANSFORMER FOR THE STUDY OF RADIAL DEFORMATION

Degree of Deformation	Capacitance $\left[\frac{nF}{\text{unit of the length of the winding}}\right]$		
	Finite Element Method	Analytical Calculation	
Without Deformation	0.5886	Plate Capacitor $(\varepsilon_0\varepsilon_r\frac{A}{d})$	0.5898
		Cylinder Capacitor $(\frac{2\pi\varepsilon_0\varepsilon_r}{\ln\frac{r_o}{r_i}})$	0.5877
Degree 1	0.6192	0.6173	
Degree 2	0.6593	0.6568	
Degree 3	0.6998	0.6962	
Degree 4	0.7387	0.7356	

winding for deformed test transformer. For example 360 section capacitances of the plate capacitors can be summed as:

$$C_i = \sum_{k=1}^{k=360} c_k. \quad (6)$$

The calculated capacitance between two windings with different deformation degrees are given in Table II. With the calculation of the capacitance without deformation of the turns, Table II shows that the calculation with plate capacitor has only a small deviation in comparison to the cylindrical condenser calculation. The results of finite element method in Table II show the accuracy of calculations with (6).

The longitudinal capacitance K_i presents electrostatically stored energy between the turns of a winding unit, and is difficult to be calculated analytically. An approximation is the assumption of a linear voltage distribution along a winding unit [19], [20].

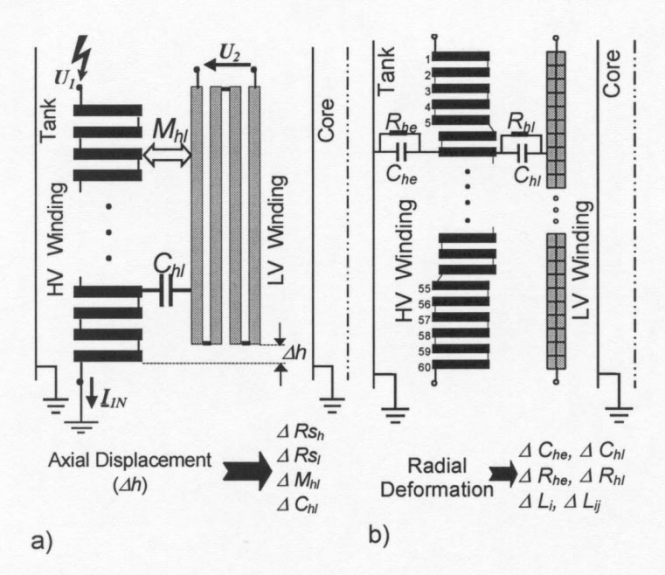

Fig. 8. Influence of mechanical displacement on parameters of the model: (One) axial displacement, (Two) radial deformation.

C. Resistances

Electric and magnetic behavior of transformer windings are subject to the damping mechanisms due to:

- *Core losses* (hystersis and eddy current in core)
- *Losses in windings and insulations* (direct current losses in turns, eddy current losses in turns and dielectric losses)

At higher frequencies (>10 kHz for power transformers) the magnetic penetration depth is so low that the core losses can be neglected. Rs_i represents the conductor resistance with skin and proximity effects. Rp_i and Re_i represent the dielectric losses between winding turns and between winding and tank (or other windings or core) respectively, and both of them are frequency dependent. The calculation of these resistances is explained thoroughly in [19], [21], [22]. In order to analyze the model in the time domain with frequency dependent resistances, an equivalent circuit for the representation of this phenomena has to be found [23].

IV. Parameter Changes of the Model Due to Mechanical Displacements

In the case of an axial displacement Δh, a change in the magnetic and electric fields can be observed. For the model, which is depicted in Fig. 4, this results in a deviation of the series resistances Rs_i in both windings. As shown in Fig. 8(a), variations in the magnetic and electrical field affect additionally the mutual inductance M_{hl} between the units of the double disk winding and the units of the layer winding as well as the parallel capacitance C_{hl} between the units of two windings.

The distribution of the magnetic field is different along the windings. It is approximately uniform in the middle of the windings and irregular at the beginning and the end of the windings. Therefore, the changes of series resistances Rs_i are different for each unit. Fig. 9 shows these changes for units of the double disk winding resulting from axial displacements. The resistance

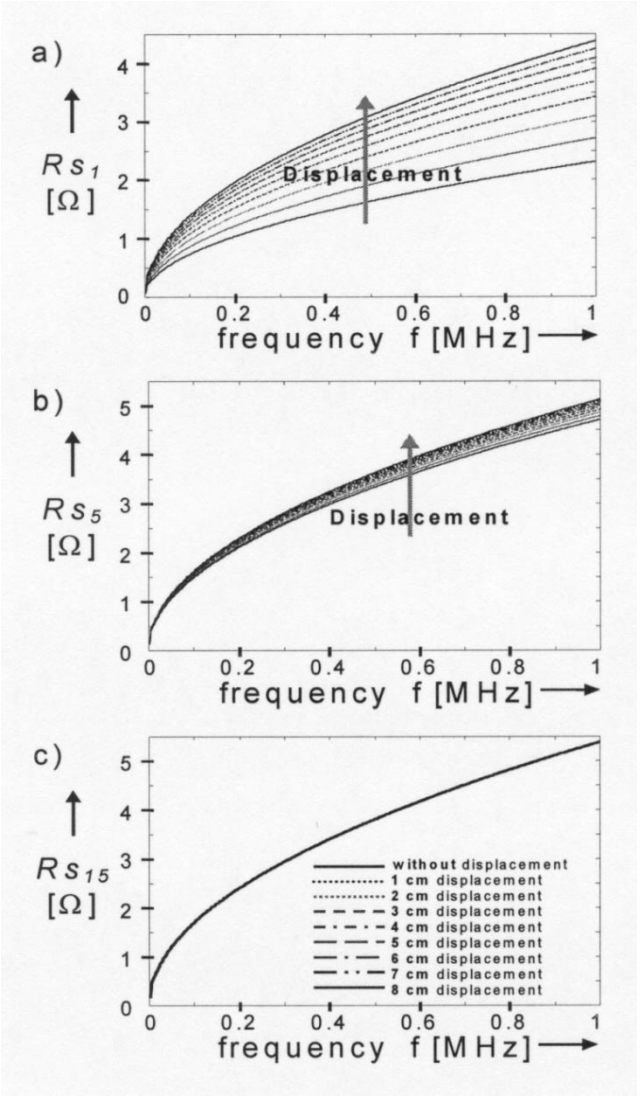

Fig. 9. Series resistances of double disk winding units (each unit contains one double disk): (One) first unit (at the beginning of the winding), (Two) 5th unit, (Three) 15th unit (in the middle of the winding).

of the first unit increases more with the displacement than the resistance of the fifth unit. The middle unit has almost a constant resistance. The resistance of the units of the second half of the winding decreases with the displacement.

The axial displacement changes the elements of the inductance matrix that describe the mutual inductance between units of one winding and units of the other winding. For example, the mutual inductance between the sixth unit of the double disk winding and the first unit of the layer winding is given in Table III for different displacements.

In the case of radial deformation, a change in the magnetic and electric fields can be observed, too. Fig. 8(b) illustrates the variations of parameters in the deformed winding. Table II shows an example of the changes of capacitance in the case of radial deformation.

The inductance matrix in the deformed case is a 53×53 matrix, which considers 53 winding units. The elements from 1 to 30 represent the high voltage winding, in which the elements from 4 to 27 describe the deformed units. The elements from 31

TABLE III
MUTUAL INDUCTANCE BETWEEN THE SIXTH UNIT OF THE DOUBLE DISK WINDING AND THE FIRST UNIT OF THE LAYER WINDING

Displacement (cm)	Mutual inductance (μH)
0	13.4858
1	12.3061
2	11.2041
3	10.1916
4	9.2704
5	8.4370
6	7.6852
7	7.0080
8	6.3983

to 53 describe the low voltage winding. Some typical elements of the inductance matrix are given in Table IV.

TABLE IV
SOME TYPICAL ELEMENTS OF INDUCTANCE MATRIX OF THE TEST TRANSFORMER FOR THE STUDY OF RADIAL DEFORMATION

Inductance (μH)	Degree of Deformation				
	Without Deformation	Degree 1	Degree 2	Degree 3	Degree 4
$L_{2,4}$	122.5301	122.1686	121.7428	121.3169	120.8911
$L_{2,10}$	24.2021	24.0881	23.9626	23.8371	23.7116
$L_{2,20}$	4.1953	4.1609	4.1336	4.1064	4.0791
$L_{6,6}$	276.9438	275.3246	273.7391	272.1564	270.5713
$L_{6,7}$	188.0966	186.8225	185.6377	184.4555	183.2711
$L_{6,10}$	66.2699	65.7208	65.1785	64.6385	64.0965
$L_{6,20}$	7.9077	7.8091	7.7120	7.6168	7.5198
$L_{6,33}$	4.6534	4.6325	4.6009	4.5693	4.5377
$L_{6,43}$	0.2995	0.2977	0.2960	0.2943	0.2927
$L_{6,53}$	0.0494	0.0489	0.0486	0.0482	0.0479

V. MATHEMATICAL REPRESENTATION OF THE DETAILED MODEL

Without considering the inductive branches in Fig. 4, the elements of the admittance matrix $\underline{\boldsymbol{Y}} = \boldsymbol{G} + j\omega\boldsymbol{C}$ can be described as follows:

$\underline{Y}_{ii}$ = The sum of admittances, which are connected to the node i

$\underline{Y}_{ij}$ = Negative sum of the admittance between nodes i and j

The inductive branches can be considered with the impedance matrix $\underline{\boldsymbol{Z}} = \boldsymbol{R} + j\omega\boldsymbol{L}$: See equation (7) at the bottom of the page.

The variables are the vectors $\underline{\boldsymbol{U}}$ and $\underline{\boldsymbol{I}}$, respectively the node voltage vector $(nv \times 1)$ and the branch current vector $(ni \times 1)$. Based on Kirchhoff's laws the following equations can be written:

$$\boldsymbol{YU} = \boldsymbol{AI} + \boldsymbol{B_1} \tag{8}$$

$$\underline{\boldsymbol{ZI}} = \boldsymbol{A}^T\underline{\boldsymbol{U}} + \underline{\boldsymbol{B_2}}. \tag{9}$$

The input is given in the vectors $\underline{\boldsymbol{B_1}}\,(nv \times 1)$ and $\underline{\boldsymbol{B_2}}\,(ni \times 1)$. $\boldsymbol{A}$ is the incidence matrix and has the elements of 0,1, -1.

The solutions of the equations mentioned above are:

$$\underline{\boldsymbol{U}} = (\underline{\boldsymbol{Y}} + \boldsymbol{A}\underline{\boldsymbol{Z}}^{-1}\boldsymbol{A}^T)^{-1}(\boldsymbol{A}\underline{\boldsymbol{Z}}^{-1}\underline{\boldsymbol{B_2}} + \underline{\boldsymbol{B_1}}) \tag{10}$$

$$\underline{\boldsymbol{I}} = \underline{\boldsymbol{Z}}^{-1}(-\boldsymbol{A}^T\underline{\boldsymbol{U}} + \underline{\boldsymbol{B_2}}). \tag{11}$$

$\underline{U}_i$ and $\underline{I}_i$ represent the Fourier transforms of the voltages and the currents for each winding unit. Corresponding time domain signals can be determined by means of IFFT (inverse fast Fourier transformation). Transfer functions are the quotient of corresponding voltage and current phasors. Any irregularities or deformations of the winding will affect both impedance matrix and admittance matrix.

The state space representation of the above mentioned equations results in:

$$\frac{d}{dt}\boldsymbol{X}(t) = \boldsymbol{S}\boldsymbol{X}(t) + \boldsymbol{B}\boldsymbol{r}(t) \tag{12}$$

with state vector

$$\boldsymbol{X}(t) = [u_1\ \ldots\ u_{nv}\, i_1\ \ldots\ i_{ni}]^T \tag{13}$$

and $r(t)$ as the input signal. $\boldsymbol{B}$ is called the input vector. The system matrix S is calculated as follows:

$$\boldsymbol{S} = \begin{bmatrix} -\boldsymbol{C}^{-1}\boldsymbol{G} & \boldsymbol{C}^{-1}\boldsymbol{A} \\ -\boldsymbol{L}^{-1}\boldsymbol{A}^T & -\boldsymbol{L}^{-1}\boldsymbol{R} \end{bmatrix}. \tag{14}$$

$\boldsymbol{L}$ is the imaginary part of $\underline{\boldsymbol{Z}}$ divided by ω (angular frequency), $\boldsymbol{C}$ is the imaginary part of $\underline{\boldsymbol{Y}}$ divided by ω, and $\boldsymbol{R}$ and $\boldsymbol{G}$ are respectively the real part of $\underline{\boldsymbol{Z}}$ and the real part of $\underline{\boldsymbol{Y}}$.

The resonance frequencies of the transformer winding are the imaginary part of the eigenvalues of this matrix.

$$f_{\text{resonance}} = \operatorname{Im}\left(\frac{Eig(\boldsymbol{S})}{2\pi}\right). \tag{15}$$

VI. COMPARISON OF MEASUREMENTS AND CALCULATIONS

The transfer functions of the transformer shown in Fig. 8(a) are defined as follows:

$$\underline{TF}_{1N}(f) = \frac{\underline{I}_{1N}(f)}{\underline{U}_1(f)} \tag{16}$$

$$\underline{TF}_{U2}(f) = \frac{\underline{U}_2(f)}{\underline{U}_1(f)}. \tag{17}$$

As an example, the calculated and measured transfer function of the earth current $\underline{I}_{1N}$ for the test object of Fig. 8(a) are given in Fig. 10. The phase of the transfer functions do not contain additional information [5] and therefore is not discussed in this paper.

$$\underline{Z} = \begin{bmatrix} Rs_1(\omega) + jL_1\omega & jL_{1,2}\omega & \ldots & jL_{1,n}\omega \\ jL_{2,1}\omega & Rs_2(\omega) + jL_2\omega & \ldots & jL_{2,n}\omega \\ \ldots & \ldots & \ldots & \ldots \\ jL_{n-1,1}\omega & jL_{n-1,2}\omega & \ldots & jL_{n-1,n}\omega \\ jL_{n,1}\omega & jL_{n,2}\omega & \ldots & Rs_n(\omega) + jL_n\omega \end{bmatrix}. \tag{7}$$

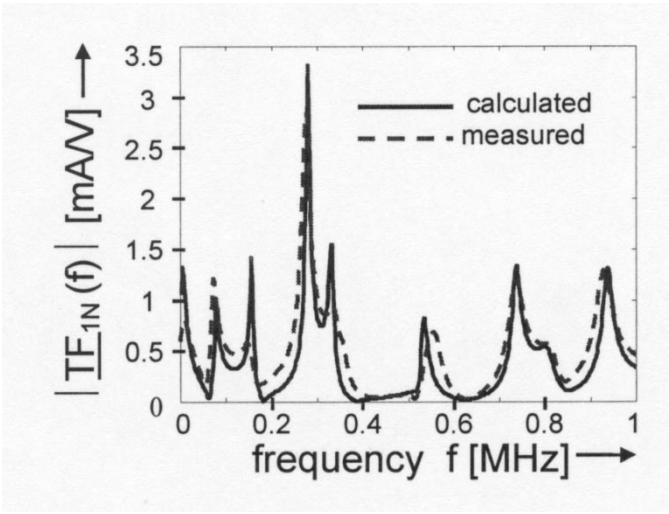

Fig. 10. Comparison of measured and calculated transfer function of the earth current $\underline{I}_{1N}$ Fig. 8(a).

The good agreement of the calculated and measured results confirms the suitability of the used model. The deviations between the measurement and the calculation (Fig. 10) can be explained by:

- Using lumped elements for the presentation of distributed electric and magnetic field behavior,
- Cable damping, transient characteristic of sensors, etc., can result in some effects, which are not considered in the model,
- Manufacturing tolerances and parameter dispersions of a real winding arrangement.

The resonance frequencies can also be calculated directly from (15). Although $\boldsymbol{R}$ and $\boldsymbol{G}$ in (14) are frequency dependent, the results in Table V show that there is only a small difference in the calculated resonance frequencies with the $\boldsymbol{R}$ and $\boldsymbol{G}$ values taken at 1 MHz (case A) and at 50 Hz (case B).

The comparison between resonance frequencies in Table V and Fig. 10 shows that the two quite near frequencies (531 and 537 kHz) overlap and the resonance at 406 kHz has a very small magnitude and cannot be seen in Fig. 10. Therefor, it is recommended to study the resonance frequencies not only in a graphical but also in a tabular form (Table V and Fig. 10).

Fig. 11 shows the results of the calculations and the measurements of the transfer functions (case Fig. 3(b)) with the different axial displacements of the four layer winding. The accuracy for the determination of the transfer functions in the time domain is limited due to the digitalization and the band limitation of the exciting signal. Considering this accuracy problem, a sensitivity limit of approx. 1 cm can be determined for the measured transfer functions. This is about 1.2% of the axial height of the winding.

The agreement of the measurements and the calculations shows that the tendency of the changes is modeled correctly. The best agreement in the case of the earth current is at about 510 kHz and in the case of the transferred voltage at 560 kHz. In addition, Fig. 11 shows that the sensitivity of the method is not good for the frequency range below 200 kHz. This fact is verified by the computer model, too.

TABLE V
RESONANCE FREQUENCIES: (1ST) $\boldsymbol{R}$ AND $\boldsymbol{G}$ CALCULATED AT 1 MHZ. (2ND) $\boldsymbol{R}$ AND $\boldsymbol{G}$ CALCULATED AT 50 HZ

Resonance number	Resonance frequencies [*kHz*] (A)	Resonance frequencies [*kHz*] (B)
1	77.87	77.82
2	156.12	156.10
3	280.23	280.17
4	331.98	331.55
5	406.98	408.56
6	531.09	530.91
7	537.79	537.88
8	737.84	737.72
9	809.02	808.82
10	939.28	939.20

The effect of changing each parameter on transfer functions has been studied separately. These studies show that the C_{hl} changes have an unimportant effect on the results and can be neglected for the simulation of axial displacements.

Fig. shows the results of the calculations and the measurements of the transfer functions (case Fig. 3(b)) with the different degree of radial deformation of the double disk winding defined in Table I. These results show that the radial deformation affected the entire frequency domain. The study of the effect of modifications of each parameter on the transfer function shows that changes in the inductance matrix in the case of radial deformation can be neglected. This can be seen in all transfer functions. As an example the transfer function of the earth current is shown in Fig. 13.

Two types of radial deformation have been performed. The simulated radial buckling affects the outer HV coil. This kind of deformation is not typical for high current faults. Rough transportation or nonprofessional repair is able to affect this kind of damage. The absolute sensitivity is of about 1 cm radial depth and of an axial extension of 86% at two $\delta/2$-sections. Short circuit faults usually affect the inner LV coil. A second investigation of a radial buckling at a LV layer winding shows a sensitivity of 1 cm radial depth at an axial extension of 10% of the coils height.

The transfer function measurements have been done with different measurement setups (Fig. 3). To compare the sensitivity of each transfer function measuring method, the relative deviation of the frequency and amplitude has been defined as follows:

$$\frac{\ddot{A}f_i}{f_i} = \left(\frac{f_{k,i} - f_{o,i}}{f_{o,i}}\right) \tag{18}$$

$$\frac{\ddot{A}A_i}{A_i} = \left(\frac{A_{k,i} - A_{o,i}}{A_{o,i}}\right). \tag{19}$$

$f_{o,i}$ i-th resonance frequency in normal condition
$A_{o,i}$ Magnitude of i-th resonance frequency in normal condition
$f_{k,i}$ i-th resonance frequency with axial displacement of k cm or radial deformation of degree k
$A_{k,i}$ magnitude of i-th resonance frequency with axial displacement of k cm or radial deformation of degree k

The evaluation of the results shows that:

- All transfer functions have approximately the same sensitivity to an axial displacement or to a radial deformation in the case of the used test objects.

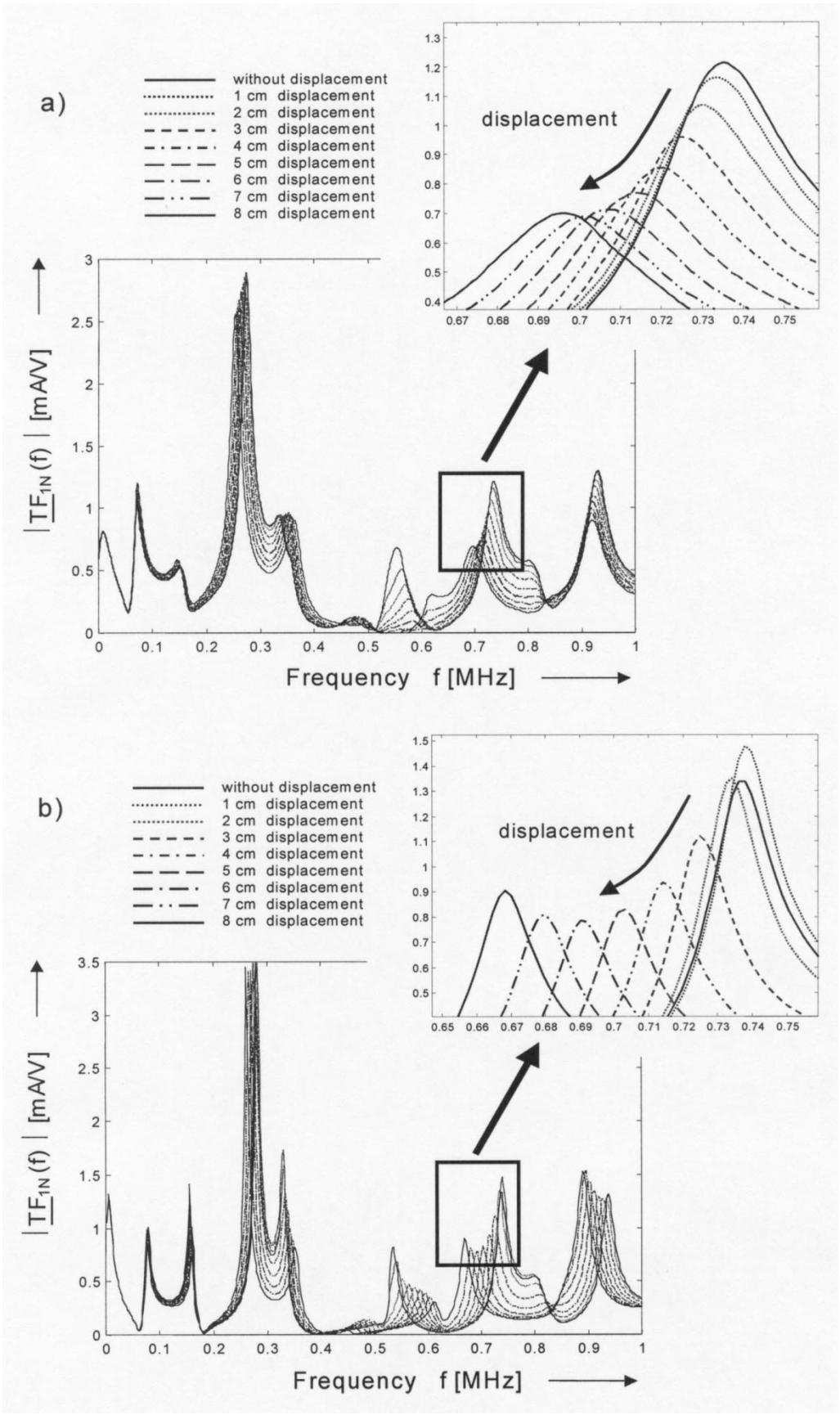

Fig. 11. (a,b). Comparison between measurement and calculation for the sensitivity analysis of axial displacement of winding (One) measured transfer function of earth current, (b) calculated transfer function of earth current.

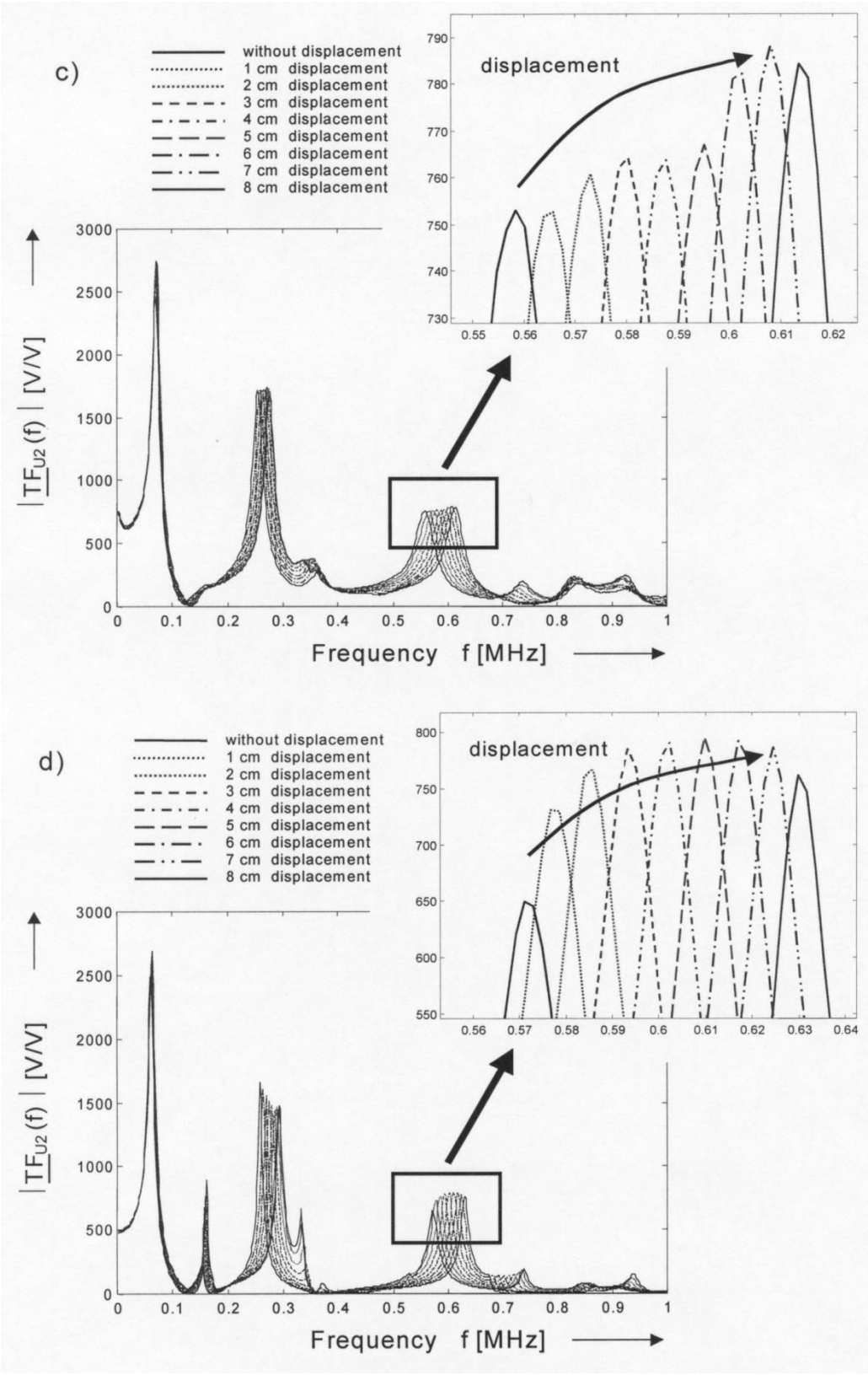

Fig. 11. (c,d). Comparison between measurement and calculation for the sensitivity analysis of axial displacement of winding, (c) measured transfer function of transferred voltage, (d) calculated transfer function of transferred voltage.

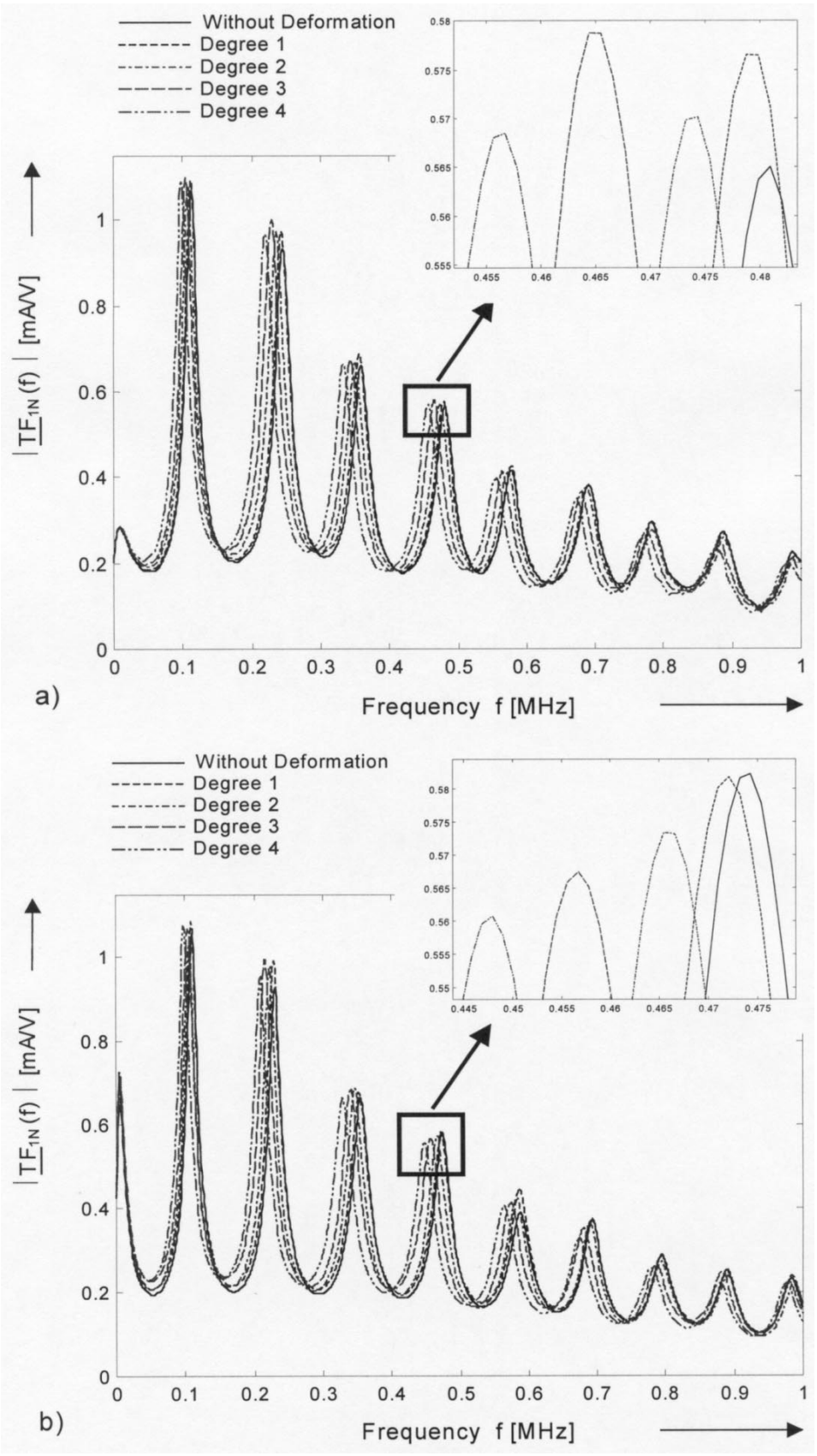

Fig. 12. (a,b). Comparison between measurement and calculation for the sensitivity analysis of radial deformation of winding (one) measured transfer function of earth current. (b) Calculated transfer function of earth current.

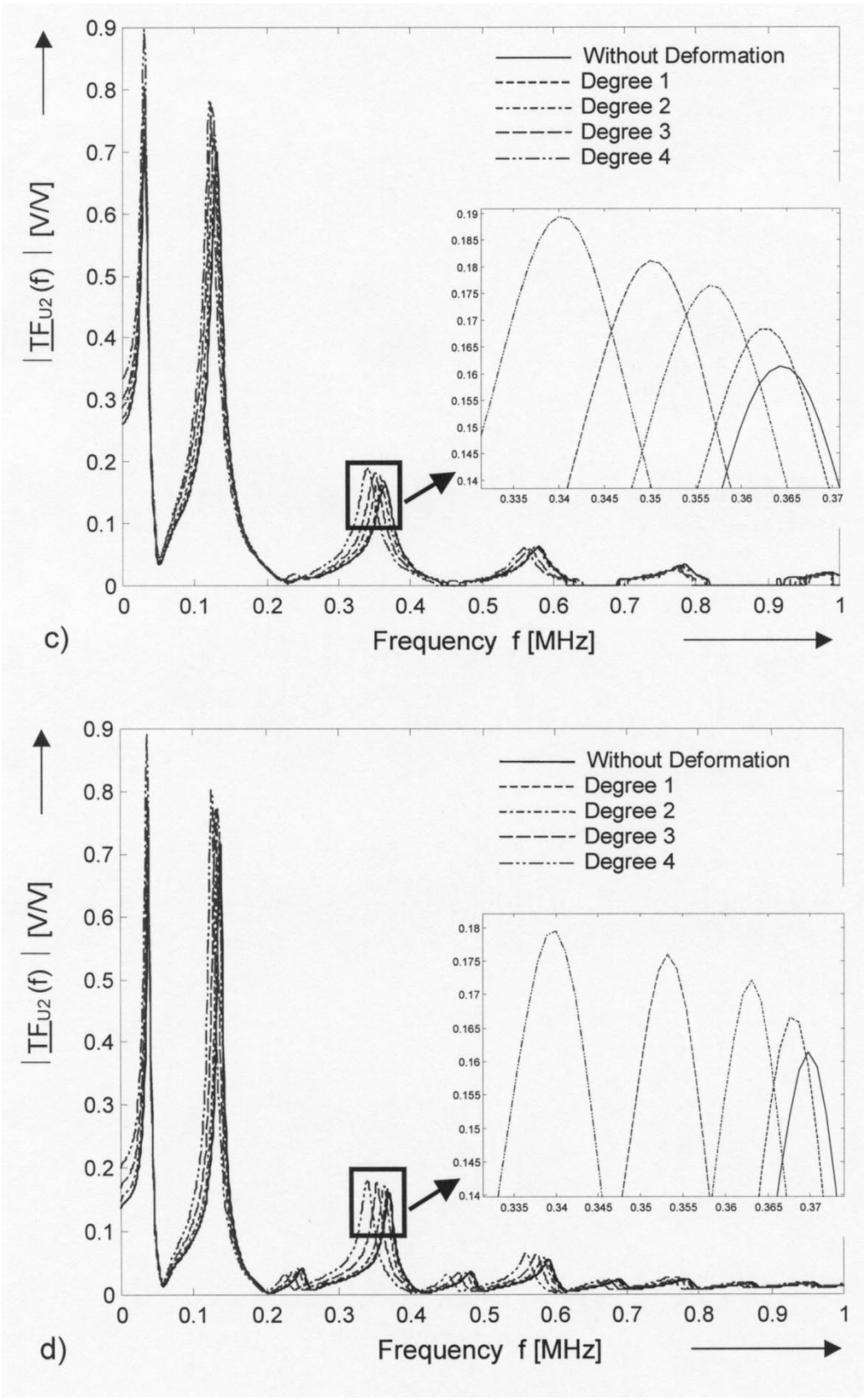

Fig. 12. (c,d). Comparison between measurement and calculation for the sensitivity analysis of radial deformation of winding. (c) Measured transfer function of transferred voltage. (d) Calculated transfer function of transferred voltage.

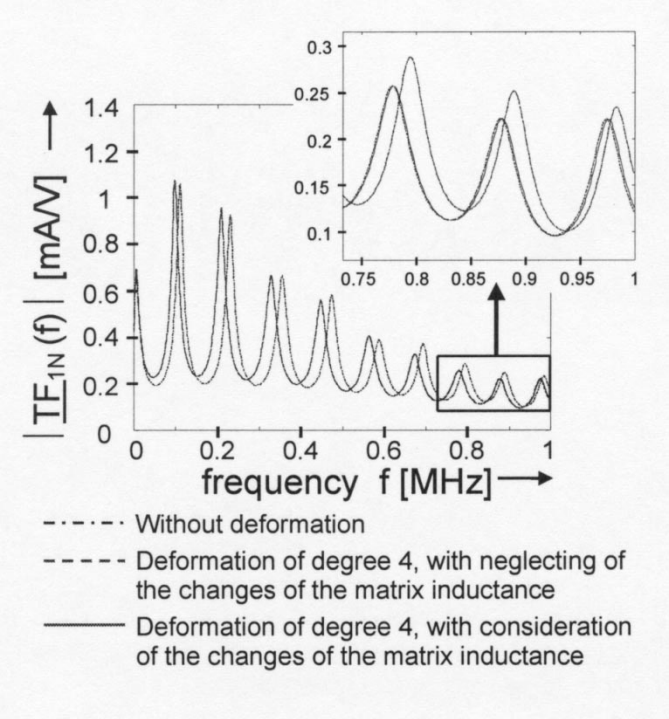

Fig. 13. Influence of the inductance matrix on the transfer function of the earth current in the case of radial deformation.

- Some of the poles in a transfer function are more sensitive than others to an axial displacement. Due to resolution restrictions, the use of high pass filters (for example with approximately 200 kHz cutoff frequency in this investigation) is recommended in the case of the study of axial displacement, especially for transfer functions that have a larger amplitude in low frequencies.
- Approximately all of the resonance frequencies have the same sensitivity to the radial deformation of the winding in the used test object.
- The agreement between the measured and calculated deviations of frequencies and amplitudes is very good.

To generalize the shown results is quite uncertain. The used assemblies behave like transfer lines. This is unusual for interleaved coils of big power transformers. The most obvious visibility of mechanical damages can be detected in the characteristics of dominant resonances. If there is one in the concerned frequency range, there will be a satisfactory sensitivity for the damage, according to the presented results. Up to now there are no experience related to rectangular transformers. All tested objects include round coils.

VII. Conclusions

In this paper the ability of the detailed model for the detection of axial displacement and radial deformation of windings and their mathematical descriptions in the frequency domain are evaluated and correlated with experimental results on two test transformers. It is shown that:

— There is a good agreement between measured and calculated results in the frequency range of a few kHz to 1 MHz. The model predicts the essential frequency characteristics (resonant frequencies and damping of a resonance) correctly.

— The correlation between changes of the transfer function and the correspondent axial displacements and radial deformations is given correctly by the model. These results prove that the mechanical displacements in transformer windings can be examined with the help of the detailed model.

— All transfer functions show that the radial deformation changes the transfer function characteristics in the entire frequency range whereas the axial displacement changes them above approximately 200 kHz.

— The changes of capacitance can be neglected in the model for the axial displacement studies and the changes of inductance matrix can be neglected for the radial deformation studies.

— The terminal conditions cannot change the resonance behavior significantly.

— Resonance frequencies which are highly sensitive to the mechanical displacements are different in the different transfer functions.

References

[1] T. Leibfried and K. Feser, "Monitoring of power transformers using the transfer function method," *IEEE Trans. Power Delivery*, vol. 14, pp. 1333–1341, Oct. 1999.

[2] K. Feser, J. Christian, C. Neumann, U. Sundermann, T. Leibfried, A. Kachler, and M. Loppacher, "The transfer function method for detection of winding displacements on power transformers after transport, short circuit or 30 years of service," in CIGRE 12/33-04, 2000.

[3] J. Christian, K. Feser, U. Sundermann, and T. Leibfried, "Diagnostics of power transformers by using the transfer function method," in *Proc. 11th Int. Symp. High Voltage Eng.*, vol. 1, London, U.K., Aug. 1999, pp. 37–40.

[4] P. T. M. Vaessen, "Transformer model for high frequencies," *IEEE Trans. Power Delivery*, vol. 3, pp. 1761–1768, Oct. 1988.

[5] A. Morched, L. Marti, and J. Ottewangers, "A high frequency transformer model for the EMTP," *IEEE Trans. Power Delivery*, vol. 8, pp. 1615–1626, July 1993.

[6] Y. Shibuya, S. Fujita, and N. Hosokawa, "Analysis of very fast transient overvoltage in transformer winding," *Proc. Inst. Elect. Eng..-Gener. Transm. Distrib.*, vol. 144, no. 5, pp. 461–468, Sept. 1997.

[7] E. Buckow, "Berechnung des Verhaltens von Leistungstransformatoren bei Resonanzanregung und Möglichkeiten des Abbaus Innerer Spannungsüberhöhungen," Ph.D., TH Darmstadt, Darmstadt, Germany, 1986.

[8] V. Brandwajn, H. W. Dommel, and I. I. Dommel, "Matrix representation of three-phase N-winding transformers for steady- state and transient studies," *IEEE Trans. Power Apparat. Syst.*, vol. PAS-101, pp. 1369–1378, June 1982.

[9] C. M. Arturi, "Transient simulation and analysis of a three-phase five-limb step-up transformer following an out-of-Phase synchronization," *IEEE Trans. Power Delivery*, vol. 6, pp. 196–207, Jan. 1991.

[10] P. Silvester and M. V. K. Chari, "Finite element solution of saturable magnetic field problems," *IEEE Trans. Power Apparat. Syst.*, vol. PAS-89, pp. 1642–1651, Sept./Oct. 1970.

[11] G. B. Gharehpetian, H. Mohseni, and K. Möller, "Hybrid modeling of inhomogeneous transformer windings for very fast transient overvoltage studies," *IEEE Trans. Power Delivery*, vol. 13, pp. 157–163, Jan. 1998.

[12] F. de Leon and A. Semlyen, "Complete transformer model for electromagnetic transients," *IEEE Trans. Power Delivery*, vol. 9, pp. 231–239, Jan. 1994.

[13] E. Rahimpour, J. Christian, K. Feser, and H. Mohseni, "Modellierung der transformatorwicklung zur Berechnung der Übertragungsfunktion für die Diagnose von Transformatoren," in *Elektrie*, Berlin, 2000, Paper no. 54/1-2, pp. 18–30.

[14] T. Leibfried, "Die Analyze der Übertragungsfunktion als Methode zur Überwachung des Isolationszustandes von Großtransformatoren," Ph.D., Univ. Stuttgart, Stuttgart, Germany, 1996.
[15] I. Wolff, *Maxwellsche Theorie: Grundlagen und Anwendungen*. Berlin: Springer-Verlag, 1997.
[16] A. Gray, *Absolute Measurements in Electricity and Magnetism*. New York: Dover, 1967.
[17] E. Isaacson and H. B. Keller, *Analysis of Numerical Methods*. New York: Wiley, 1971.
[18] A. Miki, T. Hosoya, and K. Okuyama, "A calculation method for impulse voltage distribution and transferred voltage in transformer windings," *IEEE Trans. Power Apparat. Syst.*, vol. PAS-97, pp. 930–939, May/June 1978.
[19] M. Nothaft, "Untersuchung der Resonanzvorgänge in Wicklungen von Hochspannungsleistungstransformatoren Mittels Eines Detaillierten Modells," Ph.D., TH Karlsruhe, Karlsruhe, Germany, 1995.
[20] G. M. Stein, "A study of the initial surge distribution in concentric transformer windings," *IEEE Trans. Power Apparat. Syst.*, vol. PAS-83, pp. 877–893, Sept. 1964.
[21] W. Dietrich, "Berechnung der wirbelstromverluste in den wicklungen von mehrwicklungstransformatoren," *ETZ-Archiv*, vol. 10, no. 10, pp. 309–317, 1988.
[22] ——, "Berechnung der wirkverluste von transformatorwicklungen unter berücksichtigung des tatsächlichen streufeldverlaufs," *Archiv Für Elektrotechnik*, vol. 46, no. 4, pp. 209–222, 1961.
[23] F. de Leon and A. Semlyen, "Time domain modeling of eddy current effects for transformer transients," *IEEE Trans. Power Delivery*, vol. 8, pp. 271–280, Jan. 1993.

Ebrahim Rahimpour was broin in 1971. He received the B.S. and M.S. degrees in electrical power engineering from Tabriz University and Faculty of Engineering of Tehran University, Iran, in 1993 and 1995, respectively. He is currently pursuing the Ph.D. degree at Tehran University.

Currently, he is with the Institute of Power Transmission and High Voltage Technology of Stuttgart University, Germany, working on modeling of transformers for the simulation of transfer functions. In 1996, he was a Lecturer with the Electrical Engineering Department of Zanjan University.

He received a German Academic Exchange Service scholarship in 1998.

Jochen Christian was born in 1969. He studied electrical engineering at the University of Stuttgart, Germany, and received the Dipl.-Ing. degree in 1996.

In 1997, he joined the Institute of Power Transmission and High Voltage Technology. The topic of his research is the transfer function method for onsite diagnosis of power transformers.

Kurt Feser (F'89) was born in 1938. He studied electrical engineering at the Technical University of Munich, Germany, and received the Dip.-Ing. and Dr.-Ing. degrees from the University of Munich in 1963 and 1970, respectively.

In 1971, he joined Haefely & Cie AG, Basel, Switzerland, as a chief development engineer. In 1980, he was a Director and Member of the executive board of Haefely, responsible for capacitors and high voltage test equipment. In April 1982, he joined the University of Stuttgart as head of the Power Transmission and High Voltage Institute.

Dr. Feser is a fellow of IEEE, member of VDE and CIGRE, chairman of IEC TC 42 "High voltage test technique" and the author of many 200 papers.

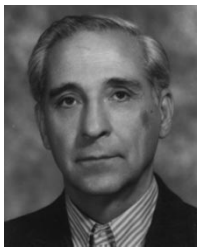

Hossein Mohseni was born in 1942. He studied electrical engineering at Technical University Graz, Austria, and received the Dipl.-Ing. and Dr.-techn. degrees in 1971 and 1975, respectively.

Currently, he is a Professor of electrical engineering and teaches High Voltage Insulation Technology and Transient in Power System and Apparatus at Tehran University. He is also a Technical Consultant with the Iran Power Generation and Transmission company (TAVANIR). From 1971 to 1976, he was a Testing and Research Engineer working in the High Voltage Laboratory and the Transformer R&D Department with ELIN Union AG, Austria. In 1976, he joined the Faculty of Engineering, University of Tehran, Iran.